TECHNICAL MEMORANDUM

832

A new hybrid formulation for the background error covariance in the IFS: implementation aspects

S. Massart

Research Department

October 2018

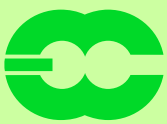

European Centre for Medium-Range Weather Forecasts
Europäisches Zentrum für mittelfristige Wettervorhersage
Centre européen pour les prévisions météorologiques à moyen terme

Series: ECMWF Technical Memoranda

A full list of ECMWF Publications can be found on our web site under:
http://www.ecmwf.int/en/research/publications

Contact: library@ecmwf.int

European Centre for Medium-Range Weather Forecasts
Shinfield Park, Reading, RG2 9AX, England

Summary

The analysis of the Integrated Forecasting System (IFS) aims at estimating the optimal model state at the initial time using all available information. The optimal state is obtained by improving the fit to the assimilated observations and to an a priori estimate of the initial state called background. This optimisation process takes account of the observation errors and the background errors.

This document focuses on the background errors. Their roles in the optimisation process are (i) to weight the background information with respect to the observation information (ii) to spatially spread the information brought by the observation (iii) to finally spread the information between the model variables. The implementation of the background errors usually combines a static part and an ensemble-based part. The ensemble-based part aims at bringing flow-dependent information while the static part acts as a regularisation of the possibly noisy information from the ensemble-based part.

Combining a static part and an ensemble-based part is already our current approach for the operational analysis. The information needed to model the ensemble-based background errors is derived from an ensemble of data assimilations (EDA). In this report, we are documenting a different approach to combine static and flow-dependent information in order to model the background errors for the analysis. The hybrid background error covariances matrix is chosen to be a weighted sum of a static matrix and an EDA-based matrix. The static matrix is based on EDA members of the past using the wavelet approach. The EDA-based matrix is computed using directly the EDA members of the day combined with a localisation function in order to reduce the noise.

The implementation of the new approach is described and the various implementation options are detailed. The new approach is illustrated through the example of the assimilation of one observation of temperature located at the beginning of the assimilation window. This framework allows to highlight the impact of the background errors. We compared several experiments using the new formulation with two reference experiments that have the same configuration but which have different background errors. The first reference experiment is based on the static background errors which is also used in the new hybrid formulation. The second reference experiment mimics the usage of the background errors of the day we have in operation. When merging the flow-dependent background errors and the static error with a respective weight of 50%/50% or 75%/25%, we show that we have an increment similar to that of the reference experiment in shape, with still a benefit from the flow dependent-information.

The single observation experiments carried on in this document do not allow to discuss the merits of the new hybrid formulation compared to the current formulation of the background error covariance. A proper comparison of the two formulations is ongoing and should help detecting the strengths and weaknesses of the current approach.

Contents

1 Introduction

The 4D-Var implementation of the Integrated Forecasting System (IFS) aims at estimating $\mathbf{x}_0^a$, the best model state at the initial time $\mathbf{x}_0$, using all available information. This is achieved by minimising the non-linear cost function

$$\mathscr{J}(\mathbf{x}_0) = \frac{1}{2}\left[\mathbf{x}_0 - \mathbf{x}^b\right]^T \mathbf{B}^{-1}\left[\mathbf{x}_0 - \mathbf{x}^b\right] + \frac{1}{2}\sum_{i=0}^{N}\left[\mathbf{y}_i - \mathbf{y}_i^o\right]^T \mathbf{R}_i^{-1}\left[\mathbf{y}_i - \mathbf{y}_i^o\right]. \tag{1}$$

The first part of the cost function of Eq. (1) computes the distance between the initial state $\mathbf{x}_0$ at time t_0 and the background state $\mathbf{x}^b$ normalised by the background error covariance matrix $\mathbf{B}$. The second part computes for each time t_i for $i \in [0,N]$ the distance between the observation vector $\mathbf{y}_i^o$ and $\mathbf{y}_i$, the model equivalent of the observation and at the same time. The distance is normalised by the observation error covariance matrix $\mathbf{R}_i$.

The model equivalent $\mathbf{y}_i$ is the propagation of the initial state $\mathbf{x}_0$ from time t_0 to time t_i with the (non-linear) forecast model M_i combined with the (non-linear) observation operator H_i,

$$\mathbf{y}_i = H_i \circ M_i(\mathbf{x}_0). \tag{2}$$

The observation operator H_i transforms the model state $\mathbf{x}_i = M_i(\mathbf{x}_0)$ at time t_i into the observation space in order to be able to compare it with the observation vector $\mathbf{y}_i^o$.

1.1 Incremental approach

In the IFS, we have an incremental approach to search for the minimum of the cost function of Eq. (1). This consists in searching for the minimums of a succession of linearised version of the cost function of Eq. (1). For this approach we introduce the control vector χ such as

$$\chi = \mathbf{B}^{-\frac{1}{2}}\delta\mathbf{x}_0 \quad \text{with} \quad \delta\mathbf{x}_0 = \mathbf{x}_0 - \mathbf{x}^b, \tag{3}$$

and then we proceed to the linearisation of the operators around the first guess state $\mathbf{x}^g$. In this document we present the case where we linearise the cost function only once. In that particular case, the first guess state $\mathbf{x}^g$ is the background state $\mathbf{x}^b$. Using the new control vector χ of Eq. (3), the model equivalent of the observation of Eq. (2) becomes

$$\mathbf{y}_i = H_i \circ M_i\left(\mathbf{x}^b\right) + \mathbf{H}_i\mathbf{M}_i\mathbf{B}^{\frac{1}{2}}\chi, \tag{4}$$

where $\mathbf{H}_i$ and $\mathbf{M}_i$ are respectively the tangent linear versions of H_i and M_i, and where the second order terms are neglected. The incremental approach allows to compute the innovation vector

$$\mathbf{d}_i^{o,b} = \mathbf{y}_i^o - H_i \circ M_i\left(\mathbf{x}^b\right), \tag{5}$$

beforehand for each time t_i. Using the new control vector of Eq. (3) and the innovation of Eq. (5) in Eq. (1) leads to the new linear cost function

$$J(\chi) = \frac{1}{2}\chi^T\chi + \frac{1}{2}\sum_{i=0}^{N}\left[\mathbf{H}_i\mathbf{M}_i\mathbf{B}^{\frac{1}{2}}\chi - \mathbf{d}_i^{o,b}\right]^T \mathbf{R}^{-1}\left[\mathbf{H}_i\mathbf{M}_i\mathbf{B}^{\frac{1}{2}}\chi - \mathbf{d}_i^{o,b}\right]. \tag{6}$$

The minimum χ^a of the new linear cost function of Eq. (6) is converted to the analysis state $\mathbf{x}^a$ with Eq. (3). In the incremental approach, the analysis state is used as a first guess around which the operators are linearised. This leads to a new linear cost function to minimise and a new minimum, which is again used to compute a new first guess, and so on. For each new linearisation of the operators, the linear version could be a simplified version of the full operator (lower resolution, simplified physics, ...).

1.2 Background errors

The control vector χ contains representations of the two and three dimensional atmospheric model variables on the model grid. If N is the size of the control vector then the background error covariance matrix has the dimension $N \times N$. With the inner loop resolution currently used, N is a large number of the order of 10^9. The background error covariance matrix is then too large to be computed and stored. It is decomposed into three main operators that can be applied sequentially: the background error correlations of the unbalanced variables ($\mathbf{C}$), the background error standard deviation (Σ^b) and the balance operator $\mathbf{K}$,

$$\mathbf{B} = \mathbf{K}\mathbf{S}_J \Sigma^b \mathbf{C} \Sigma^{b^T} \mathbf{S}_J^T \mathbf{K}^T . \tag{7}$$

In the IFS, the state $\mathbf{x}$ is a combination of atmospheric model variables in spectral space (vorticity, divergence, temperature and logarithm of surface pressure) and atmospheric model variables in grid-point space on a grid defined by a Gaussian quadrature (specific humidity and ozone). The operator $\mathbf{K}$ maps the 'unbalanced' control vector to the atmospheric model variables. The 'unbalanced' control vector is composed of vorticity (spectral space) and ozone (grid-point space) and the 'unbalanced' components of divergence, temperature and surface pressure (spectral space) and normalised relative humidity (grid-point space). The operators $\mathbf{C}$ and Σ^b operate in grid-point space. We therefore have an extra operation $\mathbf{S}_J$ in Eq. (7) that performs the spectral transform at the highest wavenumber N_J only for the variables of the 'unbalanced' control vector that are in spectral space.

If we decompose the background error correlations operator into $\mathbf{C} = \mathbf{C}^{\frac{1}{2}} \mathbf{C}^{\frac{1}{2}^T}$ in Eq. (7) and if we use Eq. (3), the change of variable becomes

$$\delta\mathbf{x}_0 = \mathbf{K}\mathbf{S}_J \Sigma^b \mathbf{C}^{\frac{1}{2}} \chi . \tag{8}$$

The computation of $\mathbf{C}^{\frac{1}{2}} \chi$ is completed using the wavelet formulation (see Appendix C of Fisher et Andersson, 2001, for more details). The wavelet form of the control vector χ is composed by a series of variables,

$$\chi = \begin{pmatrix} \chi_0 \\ \chi_1 \\ \vdots \\ \chi_J \end{pmatrix} , \tag{9}$$

where χ_j, $\forall j \in [0, J]$, is expressed in grid-point space. Each index j corresponds to a "cutoff" wavenumber N_j associated with its own reduced Gaussian grid. Table (1) gives an example of the selected wavenumbers and the associated grid.

Table 1: Example of selected wavenumbers in the wavelet approach (middle row) and number of latitudes (bottom row) for the associated reduced Gaussian grid.

Index	1	2	3	4	5	6	7	8	9	10	11	12	13
"Cutoff" wavenumber	0	1	2	3	5	7	10	15	21	31	47	63	95
Nb. of latitudes	1	1	1	1	4	8	8	16	16	32	32	64	64

For each sub-part χ_j of the control vector defined on its own reduced Gaussian grid, a vertical correlation matrix $\mathbf{C}_j$ is defined to operate on the same grid. The square root of $\mathbf{C}_j$ is then applied to χ_j and the result is transformed in the spectral space through $\mathbf{S}_j$. The wavelet formulation of the full square root of the

background error correlation is finally the sum of the contribution from each wave number j convoluted by the functions Ψ_j that defines the wavelets,

$$\mathbf{C}^{\frac{1}{2}}\chi = \mathbf{S}_J^{-1} \sum_{j=0}^{J} \Psi_j \otimes \mathbf{S}_j \mathbf{C}_j^{\frac{1}{2}} \chi_j \,. \tag{10}$$

The operator $\mathbf{S}_J^{-1}$ brings back the fields in grid-point space from the highest wavenumber N_j.

2 Hybrid background error covariance

2.1 Current hybrid background error covariance

The background error covariances are hybrid in the IFS: they are the combination of a static part and an ensemble-based part. The ensemble-based part aims at bringing flow-dependent information while the static part acts as a regularisation of the possibly noisy information from the ensemble-based part.

The ensemble information comes from the Ensemble of Data Assimilations (EDA, Bonavita *et al.*, 2012). The EDA is composed of an ensemble of 4D-Var analysis cycles at lower resolution than the deterministic 4D-Var. Each member of the ensemble makes use of perturbed observations, perturbed sea-surface temperature fields and perturbed model physical tendencies.

The background error standard deviation Σ^b of Eq. (7) is estimated using only the members from the EDA of the day and does not have a static part. The first step for its estimation is to compute the background of the unbalanced variables $\mathbf{x}_m^{ub}$, $\forall m \in [1,M]$ using the inverse of the balance operator $\mathbf{K}$,

$$\mathbf{x}_m^{ub} = \mathbf{K}^{-1}\mathbf{x}_m^b \,, \quad \forall m \in [1,M] \,. \tag{11}$$

For each element $x_{i,m}^{ub}$ of this unbalanced background vector of Eq.(11), we then compute the ensemble-mean

$$\overline{x_i^{ub}} = \frac{1}{M} \sum_{m=1}^{M} x_{i,m}^{ub} \,. \tag{12}$$

Lastly each element σ_i^b of the diagonal matrix of the background error standard deviation Σ^b is the ensemble standard deviation of the unbalanced backgrounds,

$$\Sigma^b = \begin{pmatrix} \ddots & & 0 \\ & \sigma_i^b & \\ 0 & & \ddots \end{pmatrix} \text{, where} \quad \sigma_i^b = \sqrt{\frac{1}{M-1} \sum_{m=1}^{M} \left(x_{i,m}^{ub} - \overline{x_i^{ub}} \right)^2} \,. \tag{13}$$

Note that in the IFS the background error standard deviation is computed at a fixed resolution and then interpolated in grid-point space at the inner-loop resolution.

Contrary to the background error standard deviation, the background error correlations of the unbalanced variables $\mathbf{C}$ are not computed using only the EDA members of the day. Instead the background error correlations are a combination of correlations of the day and climatological correlations. Moreover, we have to compute the square root of the correlation matrices $\mathbf{C}_j$ of Eq. (10) for all the wavenumbers N_j with $j \in [0,J]$ with the wavelet approach. For a given wavenumber N_j and using the EDA members of the day, we compute $c_j^e(k,l)$, the vertical correlation of the background error between the model levels k and l (see Appendix A). It is combined with a climatological value $c_j^s(k,l)$

$$c_j(k,l) = \alpha_j c_j^s(k,l) + (1-\alpha_j)\, c_j^e(k,l) \,, \tag{14}$$

where the coefficient α_j depends of the wavenumber. For example, $\alpha_j = 0.3$ for the small wavenumbers and up to $\alpha_j = 0.9$ for the largest wavenumbers. The computation of the climatological correlation $c^s_{k,l}$ is using EDA members of the past for several evenly sampled dates covering almost a year.

2.2 New hybrid background error covariance: design

Another approach to building a hybrid background error covariance is to compute the weighted sum of a modelled (or static) background error covariance matrix $\mathbf{B}^s$ and a background error covariance matrix $\mathbf{B}^e$ directly computed from an ensemble (Hamill et Snyder, 2000),

$$\mathbf{B}^h = \gamma^{s2}\mathbf{B}^s + \gamma^{e2}\mathbf{B}^e \quad \text{with} \quad \gamma^{s2} + \gamma^{e2} = 1\,. \tag{15}$$

In our implementation, the static background error covariance matrix $\mathbf{B}^s$ is using the same formulation as the current background error covariance matrix. The difference is that we can use climatological values instead of using the EDA members of the day to compute the standard deviation matrix Σ^b and the square root of the correlation matrix $\mathbf{C}$.

2.2.1 *Ensemble-based background error covariance*

The ensemble-based background error covariance matrix $\mathbf{B}^e$ is no longer decomposed into the operator sequence of Eq. (7). Instead it is based on an estimation of the error computed directly from an ensemble of M background states $\mathbf{x}^b_i$,

$$\widetilde{\mathbf{B}^e} = \frac{1}{M-1}\sum_{m=1}^{M}\left(\mathbf{x}^b_m - \overline{\mathbf{x}^b}\right)\left(\mathbf{x}^b_m - \overline{\mathbf{x}^b}\right)^T \quad \text{with} \quad \overline{\mathbf{x}^b} = \frac{1}{M}\sum_{m=1}^{M}\mathbf{x}^b_m\,. \tag{16}$$

If we define the perturbations of the member m by the column vector

$$\mathbf{x}^{b'}_m = \frac{1}{\sqrt{M-1}}\left(\mathbf{x}^b_m - \overline{\mathbf{x}^b}\right)\,, \tag{17}$$

and the rectangular matrix

$$\mathbf{X}^{b'} = \left(\mathbf{x}^{b'}_1 \cdots \mathbf{x}^{b'}_M\right)\,, \tag{18}$$

then the matrix $\widetilde{\mathbf{B}^e}$ is given by

$$\widetilde{\mathbf{B}^e} = \mathbf{X}^{b'}\mathbf{X}^{b'T}\,. \tag{19}$$

2.2.2 *Decomposition of the hybrid background error covariance*

To illustrate the characteristics of each part of the hybrid background errors of Eq. (15), we computed the standard deviation and the covariance at a given point for the static and ensemble-based temperature background errors for the analysis of 1 November 2017 and for the model level around 900 hPa. The ensemble-based statistics are computed from a 25 members EDA for that date.

The standard deviation of the static part of the background errors $\mathbf{B}^s$ is the square root of the mean background error variance over the period that spans between November 2017 and January 2018. With the wavelet formulation, we do not have a direct access to the background error horizontal correlation. It

is nevertheless possible to diagnose its structure using a Legendre transform (Rochas et Courtier, 1992) and then to estimate its length-scale. To estimate the covariance at a given point, we therefore multiplied the variance field by a normalised Gaussian function centered around that point and with the estimated length-scale at that point.

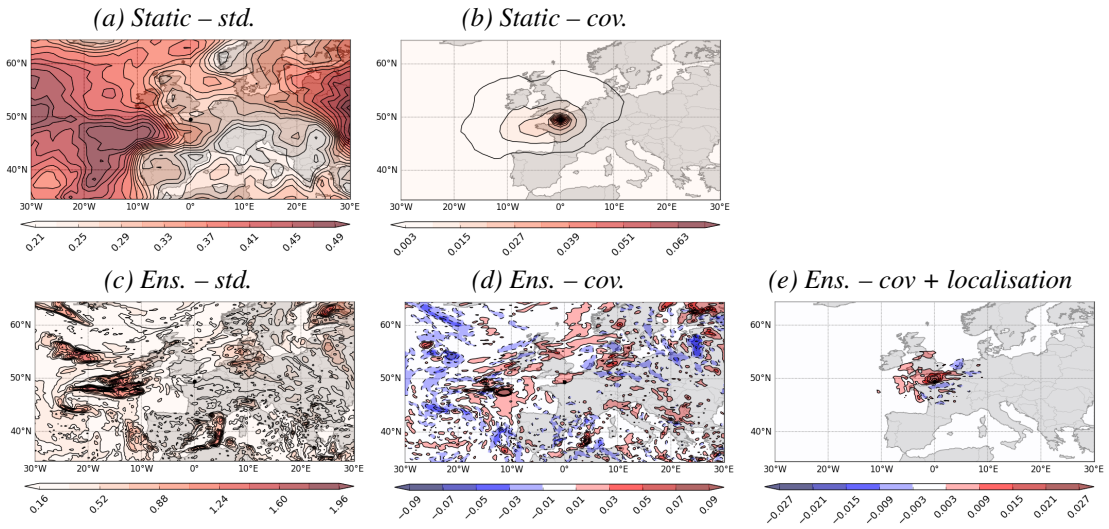

Figure 1: Examples of temperature background error statistics around 900 hPa *on 31 October 2016 at 21:00: standard deviation (a and c, in* K*) and covariance (b and d, in* K^2*) or localised covariance with a length-scale of 300* km *(e) for the point located at (50°N, 0°E). Top row: static background error. Bottom row: ensemble-based background error.*

Figure 1 displays the statistics for the static and ensemble-based temperature background errors for the analysis on 1 November 2016. The standard deviation of the static error is smooth with largest values west of France (Fig. 1a). The covariance for a point located in the middle of the English Channel (50°N, 0°E) is well-centred around the point but not isotropic by construction. It has highest values slightly to the west due to the largest values in the standard deviation (Fig. 1b).

The standard deviation of the temperature background errors of the day estimated from the ensemble is less smooth than the standard deviation from the static errors as expected (Figs. 1a and 1c). This is partially due to the sampling noise. It is also worth noting that the errors of the day are extracted and plotted on a $0.2° \times 0.2°$ regular grid while the static errors are extracted and plotted on a $1.25° \times 1.25°$ regular grid. This last grid is the closest regular grid to the T159 grid used in the current configuration for Σ^b. The truncation towards this coarser grid also smooth the static errors.

The maximum of the standard deviation of the day is located south of Iceland (Fig. 1c). With values over 2 K, the maximum is much larger than everywhere else and much larger than the maximum of the static standard deviation errors (around 0.6 K). As a consequence, the covariance for the same point as before has large values south of Iceland but also larger positive and negative values elsewhere (Fig. 1d).

2.2.3 Localisation

One expects a background error covariance to have decreasing values when moving away from the point where the covariance is computed. The previous example illustrated that this is the case with the static covariances (Fig. 1b) but not for the ensemble-based one (Fig. 1d). This issue is addressed using a

localisation that consists in applying a correlation function centred around the point where the covariance is computed.

If $\widehat{\mathbf{C}}$ is the localisation matrix that provides a correlation function for every point of the raw ensemble-based background error covariance matrix $\widetilde{\mathbf{B}^e}$ of Eq. (16), then the localised background error covariance matrix is

$$\mathbf{B}^e = \widetilde{\mathbf{B}^e} \circ \widehat{\mathbf{C}}, \tag{20}$$

where $\widehat{\mathbf{C}}$ has the same size as $\widetilde{\mathbf{B}^e}$ and $\circ$ denotes the element-by-element product of the two matrices (also called the Hadamard-Schur product).

The localisation we choose here for illustration is a Gaussian function centred around the point where we compute the covariance and with a length-scale of 300 km. When applied to the raw covariance, this localisation gives a filtered covariance field that has the desired properties (Fig. 1e). Compared to the static covariance, the filtered covariance of the day has lower values and extends more towards the north-west of the point.

2.2.4 *Hybrid weight*

To further illustrate the effect of merging static and flow dependent information in the background errors, we computed the hybrid covariance for the same point (middle of the English Channel, 50°N, 0°E) for various weights and for the temperature around 900 hPa on 31 October 2016 at 21:00 (Fig. 2).

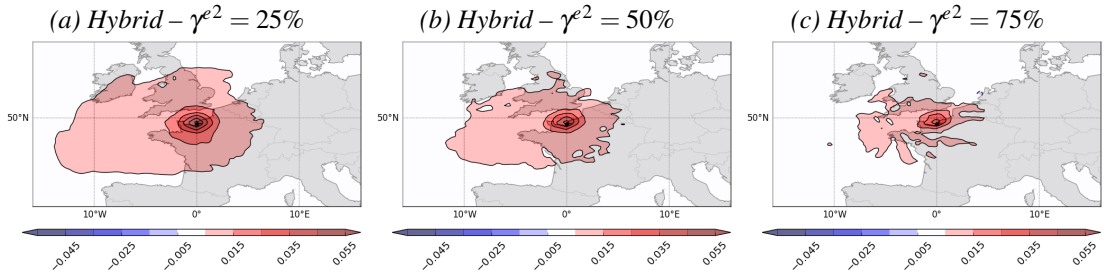

Figure 2: Example of hybrid temperature background error covariance (in K^2) obtained by combining the static covariance of Fig. (1b) and the localised ensemble-based covariance of Fig. (1e) for different weights.

In that example the hybridisation has for consequence to first decrease the amplitude of the covariance with a maximum value lower and lower when the ensemble weight γ^{e2} increases. Secondly the shape gets more and more small scale structures.

2.3 New hybrid background error covariance: implementation

2.3.1 *Algorithm*

As detailed in Section. 1.1, the IFS is using the square-root of the background error covariance matrix. To implement the hybrid background errors in that context, we choose a variation of algorithm (1) from Desroziers *et al.* (2014). The hybrid control vector χ^h is based on the current control vector (referred hereafter to as χ^s) augmented with M variables χ^e_m, $\forall m \in [1,M]$, where M is the number of used EDA

members and all having the same size as the perturbation $\mathbf{x}^{b'}_m$,

$$\chi^h = \begin{pmatrix} \chi^s \\ \chi^e \end{pmatrix} \quad \text{and} \quad \chi^e = \begin{pmatrix} \chi^e_1 \\ \chi^e_2 \\ \vdots \\ \chi^e_M \end{pmatrix}. \tag{21}$$

The expression of the cost function with the hybrid control vector remains the same as in Eq. (6) even if the control vector is now extended. The change of variable becomes

$$\delta\mathbf{x}_0 = \gamma^s \mathbf{B}^{s\frac{1}{2}} \chi^s + \gamma^e \mathbf{B}^{e\frac{1}{2}} \chi^e, \tag{22}$$

where the static part $\mathbf{B}^{s\frac{1}{2}}\chi^s$ is computed as in Eq. (8) using the wavelet formulation. The square-root of $\mathbf{B}^e$ can be written

$$\mathbf{B}^{e\frac{1}{2}} = \widehat{D}\widehat{C}^{\frac{1}{2}}, \tag{23}$$

with $\widehat{D}$ a diagonal matrix containing the elements of the perturbations $\mathbf{x}^{b'}_m$ of Eq. (17), such that the product of $\widehat{D}$ with any vector $\mathbf{v} = (\mathbf{v}_1\, \mathbf{v}_2 \cdots \mathbf{v}_M)^T$ is

$$\widehat{D}\mathbf{v} = \begin{pmatrix} \mathbf{x}^{b'}_1 & 0 & & \\ 0 & \mathbf{x}^{b'}_2 & 0 & \\ & 0 & \ddots & 0 \\ & & 0 & \mathbf{x}^{b'}_M \end{pmatrix} \begin{pmatrix} \mathbf{v}_1 \\ \mathbf{v}_2 \\ \vdots \\ \mathbf{v}_M \end{pmatrix} = \sum_{m=1}^{M} \mathbf{x}^{b'}_m \circ \mathbf{v}_m, \tag{24}$$

where $\mathbf{v}_m$, $\forall m \in [1,M]$, has the same size as the perturbation $\mathbf{x}^{b'}_m$.

To reduce the cost of this new formulation of the hybrid background error, we decided to have the same horizontal localisation for all variables of the (static) control vector and for all model level, and to neglect the vertical localisation. These hypotheses allow to expand the control vector with M two-dimensional fields $\tilde{\chi}^e_m$, $\forall m \in [1,M]$, instead of the M fields χ^e_m of the dimension of $\mathbf{x}^{b'}_m$ (see Appendix B for more details). Then, the ensemble-based part of the change of variable of Eq. (22) takes the final form

$$\mathbf{B}^{e\frac{1}{2}}\chi^e = \sum_{m=1}^{M} \mathbf{x}^{b'}_m \circ \Theta \widehat{C}_h^{\frac{1}{2}} \tilde{\chi}^e_m, \tag{25}$$

where $\widehat{C}_h^{\frac{1}{2}}$ localises horizontally the two-dimensional fields $\tilde{\chi}^e_m$, $\forall m \in [1,M]$, and Θ replicates the localised 2D fields on the model vertical levels and on all variables.

Until now, for all $m \in [1,M]$, χ^e_m had the dimension of the perturbation $\mathbf{x}^{b'}_m$ and $\tilde{\chi}^e_m$ had the dimension of a two-dimensional field of the perturbation. To take advantage of the wavelet formulation for modelling a correlation function in the IFS, we decided to express $\tilde{\chi}^e_m$ in the wavelet form such as $\widehat{C}_h^{\frac{1}{2}}\tilde{\chi}^e_m$ has the dimension of a two-dimensional field of the perturbation, and following Eq. (10),

$$\widehat{\mathbf{C}_h}^{\frac{1}{2}} \tilde{\chi}^e_m = \mathbf{S}_J^{-1} \sum_{j=0}^{J} \Psi_j \otimes \mathbf{S}_j c_j \tilde{\chi}^e_{m,j}, \tag{26}$$

where $\tilde{\chi}^e_{m,j}$, $\forall j \in [1,J]$, are the components of the vector $\tilde{\chi}^e_m$ and are a set of two-dimensional fields in grid point space similarly to Eq. (9),

$$\tilde{\chi}^e_m = \begin{pmatrix} \tilde{\chi}^e_{m,0} \\ \tilde{\chi}^e_{m,1} \\ \vdots \\ \tilde{\chi}^e_{m,J} \end{pmatrix}. \tag{27}$$

Note that the vertical correlation matrix $\mathbf{C}_j^{\frac{1}{2}}$ of Eq. (10) has been replaced by a scalar c_j in Eq. (26) since $\tilde{\chi}^e_{m,j}$, $\forall j \in [1,J]$ are two-dimensional fields. In that particular case, c_j and $\mathbf{S}_j$ can commute and the localisation of $\tilde{\chi}^e_m$ becomes

$$\widehat{\mathbf{C}_h}^{\frac{1}{2}} \tilde{\chi}^e_m = \mathbf{S}_J^{-1} \sum_{j=0}^{J} \Psi_j \otimes c_j \mathbf{S}_j \tilde{\chi}^e_{m,j} . \tag{28}$$

The localisation consists then of defining the appropriate spectral coefficient c_j, $\forall j \in [1,J]$.

2.3.2 *Limitations of the chosen implementation*

If χ_w is the control variable in the wavelet space for one variable and one level, and n_{3D} and n_{2D} are respectively the number of 3D and 2D variables in the 'unbalanced' control vector and n_l the number of vertical levels, then the size of the augmented hybrid control vector for an ensemble of M members is

$$\begin{aligned} \text{size}\left(\chi^h\right) &= \text{size}\left(\chi^s\right) + \text{size}\left(\chi^e\right) \\ &= \left(n_{3D}\, n_l + n_{2D}\right) \text{size}\left(\chi_w\right) + M\, \text{size}\left(\chi_w\right) \\ &= \left(n_{3D}\, n_l + n_{2D} + M\right) \text{size}\left(\chi_w\right) . \end{aligned} \tag{29}$$

In the current configuration $n_{3D} = 5$ (vorticity, unbalanced divergence, unbalanced temperature, normalised relative humidity and ozone) and $n_{2D} = 1$ (logarithm of surface pressure). For $n_l = 137$ levels, the increase in size for $M = 25$ members is about 3.6%. For $M = 50$ members the increase is about 7.3% and for $M = 150$ members the increase is about 22%. The choice of having two-dimensional variables for χ^e has thus a small overall impact on the size of the control vector.

Yet, even if there is a direct link between the size of the control vector and the global computational cost of the minimisation of the cost function, it is difficult to estimate how much more expensive would be a hybrid formulation with three-dimensional fields $\tilde{\chi}^e_m$, $\forall m \in [1,M]$. For $M = 50$ members, the size of the control vector would be about 30 times larger than the current size. It would be nevertheless possible to reduce the size using for example a coarser resolution in the wavelet space for the variables $\tilde{\chi}^e_m$. The methodologies that could be used to reduce the size are not discussed here as they are out of the scope of this document.

The implementation choice of the hybrid control vector has nevertheless several limitations. Having two-dimensional variables for χ^e means that the horizontal localisation has to be the same (i) for all atmospheric model variables and (ii) for all model levels. These two issues are treated respectively in sections 3.1.1 and 2.3.3.

The current implementation has no vertical localisation by construction (see Appendix B). Introducing a vertical localisation means having M three-dimensional fields χ^e_m, each of them of the size of χ^s. This option is not workable in terms of computational cost. Another option would be to apply the square-root of the vertical localisation $\widehat{\mathbf{C}_v}$ after the Hadamard-Schur product in Eq. (43),

$$\mathbf{B}^{e\,\frac{1}{2}} \chi^e = \widehat{\mathbf{C}_v}^{\frac{1}{2}} \sum_{m=1}^{M} x^{b'}_m \circ \Theta \widehat{C}_h^{\frac{1}{2}} \tilde{\chi}^e_m . \tag{30}$$

This formulation of the vertical localisation is not strictly correct as it is not an Hadamard-Schur product in the vertical. Instead, it smooths the increment using a product matrix-vector with a correlation matrix.

Finally we assume that the short forecasts that provide the background perturbations are able to reproduce the balance between the atmospheric model variables. This assumption could be relaxed using the

balance operator $\mathbf{K}$ in Eq. (43),

$$\mathbf{B}^{e\frac{1}{2}}\chi^e = \mathbf{K}\sum_{m=1}^{M} x_m^{ub'} \circ \Theta \widehat{C}_h^{\frac{1}{2}} \tilde{\chi}_m^e, \tag{31}$$

where $x_m^{ub'}$ is the unbalanced perturbation $x_m^{ub'} = \mathbf{K}^{-1} x_m^{b'}$, $\forall m \in [1,M]$. This option has not been investigated yet.

2.3.3 *Hybrid weight*

As previously explained, we have to assume that the horizontal localisation is the same for all the model levels. One solution to deal with this constraint is to use the hybrid formulation only for a vertical region of the atmosphere where this assumption is relevant. This can be achieved by tapering the hybrid weight γ^{e2} towards 0 outside this region.

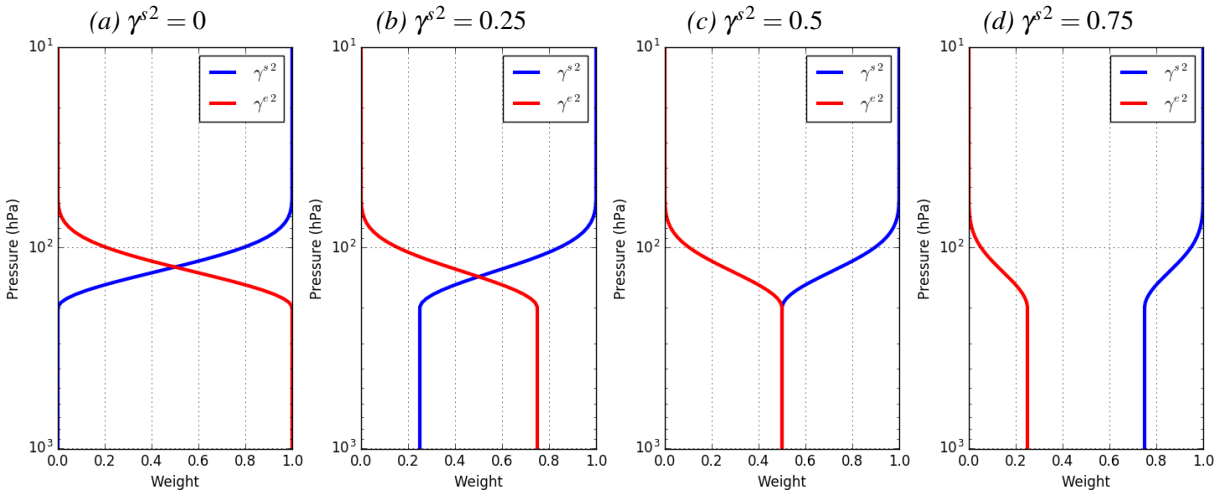

Figure 3: Examples of tapering for the hybrid weights (γ^{s2} in blue and γ^{e2} in red) when the tapering starts at 200 hPa *and finishes at 50* hPa *and for different values of γ^{s2}.*

Figure 3 presents an example of such a tapering when using the function of Eq. (4.10) from Gaspari et Cohn (1999) and when using the logarithm of the pressure as a distance. This allows, for instance, to have a hybrid formulation in the troposphere and in the boundary layer only.

3 Localisation of the background errors

In the previous section we pointed out the importance of the localisation of the background error covariance obtained from a finite number of samples in order to reduce the sampling noise. In this section we first present the estimation of the localisation length-scale for various atmospheric model variables in the control vector. We then discuss the implementation of the localisation function.

3.1 Localisation diagnostics

To estimate the localisation length-scale, we used the program *HybridDiag* developed by B. Ménétrier and presented in Ménétrier et Auligné (2015). The estimation is based on an optimal filtering of ensemble covariances that gives the best fit (Frobenius norm) to the covariance from a hypothetical infinite ensemble.

We based the estimation on 10 sets of 25 short forecasts for 25 members of an EDA. The 10 sets are randomly chosen dates in November 2016. The samples were interpolated on a regular $0.35° \times 0.35°$ horizontal grid.

3.1.1 Horizontal localisation

Figure 4a presents the estimated global length-scale of the horizontal localisation for the atmospheric model variables of the control vector for the surface up to the lower stratosphere. It shows that there is a large range of values between the variables with the minimum for the divergence and vorticity (around 50 km) and the maximum for the logarithm of surface pressure (more than 700 km).

Our implementation of the hybrid background error covariance implies that the horizontal localisation is the same for all atmospheric model variables and all model levels. The range of values found in the estimates of the horizontal localisation length-scale breaks this assumption. We thus follow an idea from Berre *et al.* (2017) that consists in applying a power of the Laplacian operator to the perturbation fields $\mathbf{x}_m^{b'}$ of Eq. (17). We found the best results by applying the Laplacian operator with different powers for the different variables: $\frac{1}{4}$ for the logarithm of surface pressure, $-\frac{1}{4}$ for the specific humidity and $-\frac{1}{2}$ for the vorticity and divergence.

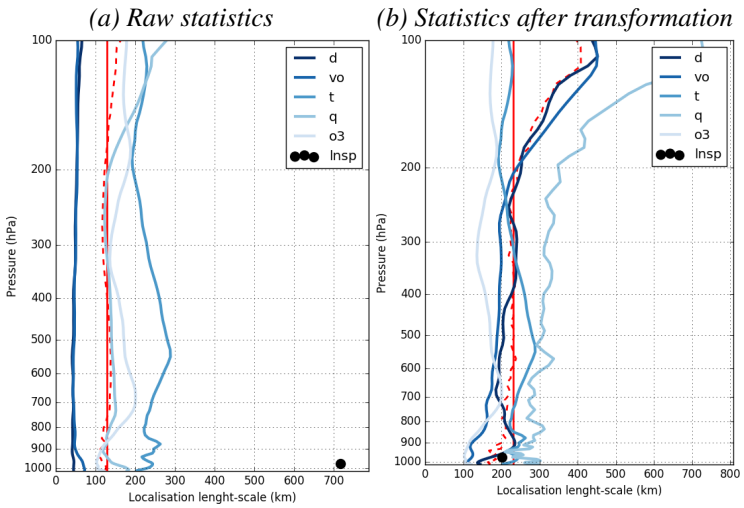

Figure 4: Profiles of the estimated horizontal localisation length-scale for the set of atmospheric model variables: (a) from 10 sets of 25 EDA members and (b) after transformation of the members (see text for details on the transformation). The length-scale for the logarithm of the surface pressure is represented by a dot. The vertical dotted red line is the profile of the averaged length-scale over the variables and the full red line is the average over the variables and model levels.

Figure 4b shows that when applying the above transformations based on the Laplacian operator to the different variables, the range of values for the length-scale of the horizontal localisation is narrower that

previously. The values are indeed mostly between 100 km and 300 km with an average around 230 km. Moreover there is not much variation of the values in the vertical. This transformation of the perturbation fields makes our implementation of the horizontal localisation possible.

Even if the diagnosed length-scale of the horizontal localisation are now closer to each other, they start to differ and increase from 200 hPa and above. This means that the ability of tapering the hybrid weight towards zeros could be useful, starting from 200 hPa.

3.1.2 Vertical localisation

Figure 5 presents the diagnosed vertical localisation length-scale from the same sample as previously and using two vertical coordinates. Using the model levels as the vertical coordinate, the length-scale values are around 2 model levels for all atmospheric model variables and from 700 hPa upwards (Fig. 5a). The length-scale for humidity has slightly larger values in the mid-troposphere. The length-scale values of all variables increase from 700 hPa to the bottom model level, with values up to 14 model levels.

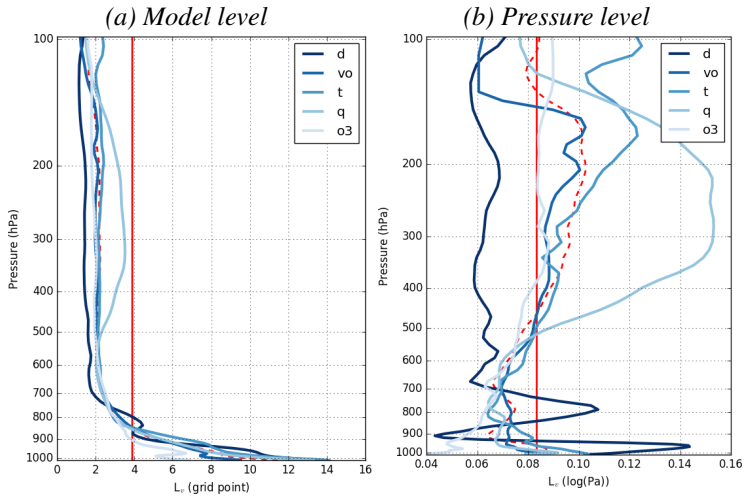

Figure 5: Profiles of the estimated vertical localisation length-scale from 10 sets of 25 EDA members and for the set of atmospheric model variables: (a) length-scale expressed as model level and (b) length-scale expressed as logarithm of pressure. The vertical dotted red line is the profile of the averaged length-scale over the variables and the full red line is the average over the variables and model levels.

Using the logarithm of pressure the vertical coordinate, the length-scale values are less homogeneous in the mid-troposphere (Fig. 5b). On the other hand there are less differences between the two regions above and below 700 hPa.

We discussed section 2.3 that our implementation does not allow the vertical localisation per se but applying a vertical localisation on the resulting increment of $\mathbf{B}^{e\frac{1}{2}}\chi^e$ is still possible. In that particular case, it would be possible to have a different localisation for each atmospheric model variable and each model level. Nonetheless, the implementation of a vertical localisation operator with the same length-scale for all variables is easier. The choice of the model level for the vertical coordinate seems better as the spread of values for the length-scales between the variables is reduced. In that case, one has to use a profile of vertical length scales.

3.2 Localisation parametrisation

We presented in section 2.3 the proposed implementation of the horizontal localisation using the wavelet formulation. We showed that we only need to specify the coefficients c_j, $\forall j \in [0,J]$, of Eq. (26). Following Weaver et Mirouze (2013), the spectral coefficients c_j, $\forall j \in [0,J]$, of an isotropic homogeneous Gaussian correlation on the sphere are

$$c_j = \frac{\gamma}{4\pi a^2}\sqrt{2j+1}\exp\left(-\frac{\kappa}{a^2}j(j+1)\right), \tag{32}$$

where the normalisation constant is

$$\gamma = 4\pi a^2\left[\sum_{j=0}^{\infty}(2j+1)\exp\left(-\frac{\kappa}{a^2}j(j+1)\right)\right]^{-1}. \tag{33}$$

The coefficient κ is the diffusion coefficient of the two-dimensional diffusion equation that represents the correlation. It is linked to Daley length-scale L_g of the Gaussian function by

$$\kappa = \frac{{L_g}^2}{2} \tag{34}$$

Figure 6 presents the horizontal localisation functions obtained with various values of L_g as diagnosed from the wavelet formulation. In this example the truncation J is the wavenumber 95. The wavelet formulation allows to well represent the Gaussian correlation function overall. The ripples in the diagnosed function for the length-scale of 150 km are due to the truncation. A truncation J at the wavenumber 95 corresponds to a regular horizontal grid of about 200 km×200 km, which is larger than the length-scale of 150 km. When the length-scale becomes larger than the horizontal grid resolution associated with the truncation, then the ripples disappear.

4 Single observation experiment

This section presents the results obtained with the new formulation for the hybrid background errors when a single observation is assimilated at the beginning of the assimilation window. We choose a temperature observation located at the same coordinates as the one used previously in the document $(50°N, 0°E)$ and at about 900 hPa. We are using the same basic settings for all the experiments presented hereafter.

The new formulation of the background errors is used only for divergence, vorticity, temperature, humidity and logarithm of surface pressure and not ozone. This choice is motivated by the fact that we are using the same variables χ^e_m, $\forall m \in [1,M]$ to multiply with the perturbations of the atmospheric model variables. We thus implicitly assume that the model variables are correctly cross-balanced for each perturbation. Ozone is weakly coupled with the other model variables through the transport and there is no dynamical nor physical feedback from ozone. For this reason we believe that the balance between ozone and the other variables may not be accurate in the model and we prefer not to use ozone in the new hybrid formulation.

The single observation experiments are all using a single outer loop at the resolution of T_{co} 399. The inner loop resolution is T_l 255. We retrieved the EDA members at the resolution of the inner loop and we

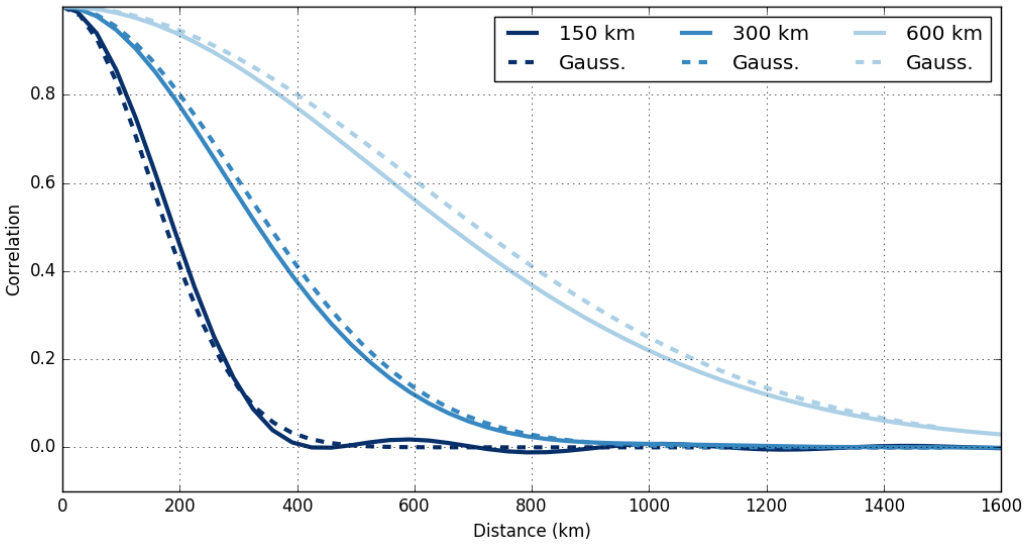

Figure 6: Example of horizontal localisation functions implemented in the wavelet formulation (solid lines) for 3 length-scales: 150 km *(dark blue), 300* km *(blue) and 600* km *(light blue). The dash lines are for the Gaussian functions of the same length-scale.*

used 25 members. In order to increase the ensemble sample and reduce the noise, we also tested tripling the ensemble size by using the ensemble members from the same EDA but with a time-lag of ± 3 hours.

The horizontal localisation uses a length-scale of 200 km and the ensemble perturbations are transformed using the Laplacian function (sec 3.1.1) unless specified otherwise. When activated, the vertical localisation operator uses a profile of vertical length-scale that comes from the mean length-scale for all the used model variables and model levels.

We are using the vertical tapering of the hybrid weight (sec. 2.3.3). It starts at 200 hPa and finishes at 100 hPa. This coincides with approximately the tropopause region. The starting pressure level corresponds to the level where the localisation statistics start to differ between the atmospheric model variables (sec. 3.1). The tapering is sharp in the pressure region between 200 hPa and 100 hPa in order to decorrelate the troposphere and the stratosphere in the hybrid formulation.

Table 2: List of the single observation experiments and details on their configuration. The first column is the name used in the document to refer to the experiment.

Exp. Name	Weight	Mem.	Vert. Loc.	Comment
STATIC	$\gamma^{e2} = 0\%$	-	-	Static background errors
HYB_100_25m	$\gamma^{e2} = 100\%$	25	off	Full flow-dependent background errors
HYB_100_75m	$\gamma^{e2} = 100\%$	75	off	Same as HYB_100_25m with more members
HYB_50_75m	$\gamma^{e2} = 50\%$	75	off	Same as HYB_100_25m with more static weight
HYB_75_75m	$\gamma^{e2} = 75\%$	75	off	Same as HYB_100_25m with more static weight
HYB_50_75m_vloc	$\gamma^{e2} = 50\%$	75	on	Same as HYB_50_75m with vertical localisation
HYB_75_75m_vloc	$\gamma^{e2} = 75\%$	75	on	Same as HYB_75_75m with vertical localisation
OPER_LIKE	-	-	-	Similar configuration as for operations

The list of the experiments we have run and we discuss hereafter is detailed in Table 2. The OPER_LIKE experiment mimics the operational setting regarding the background errors using the statistics of the day. The STATIC experiment uses background error standard deviations that have been averaged over a period of 5 months and background error correlations computed with EDA members of the past.

4.1 Initial results

For a scalar problem where the background error standard deviation is σ^b, the observation error standard deviation is σ^o and the innovation is $d^{o,b}$, the analysis increment δ^a is

$$\delta^a = \frac{\sigma^{b2}}{\sigma^{b2} + \sigma^{o2}} d^{o,b} . \tag{35}$$

In our three-dimensional framework with a single observation, this expression is a crude estimation and should be regarded as such (see Appendix C for more details). Nevertheless, it provides an insight on the expectation for the analysis increment. Using 25 members of the used EDA, we computed the background error standard deviation at the point the closest to the observation and the value is $\sigma^b = 0.19\,\mathrm{K}$. With our setting where $\sigma^o = 0.5\,\mathrm{K}$ and $d^{o,b} = -1.5\,\mathrm{K}$, the increment should be of the order of $\delta^a \approx -0.2\,\mathrm{K}$ according to Eq. (35).

For the STATIC and OPER_LIKE experiments, the computation is slightly different. Indeed, the background error standard deviation is computed from the unbalanced part of the temperature and at a different resolution: $T_l 159$ while the inner loop resolution is $T_l 255$. The unbalanced temperature background error standard deviation at the point the closest to the observation for the OPER_LIKE experiment is about $0.17\,\mathrm{K}$ and then a rescaling factor of 1.6 is apply to account for the change of resolution. This would result in an increment on the unbalanced temperature of the order of $-0.34\,\mathrm{K}$. Moreover Bonavita *et al.* (2012) showed that the balanced part of the temperature increment accounts for about 20% of the total increment, which would lead to an increment of $\approx -0.4\,\mathrm{K}$. We also rescaled the background error standard deviation of the STATIC experiment so it is similar to the one of the OPER_LIKE experiment.

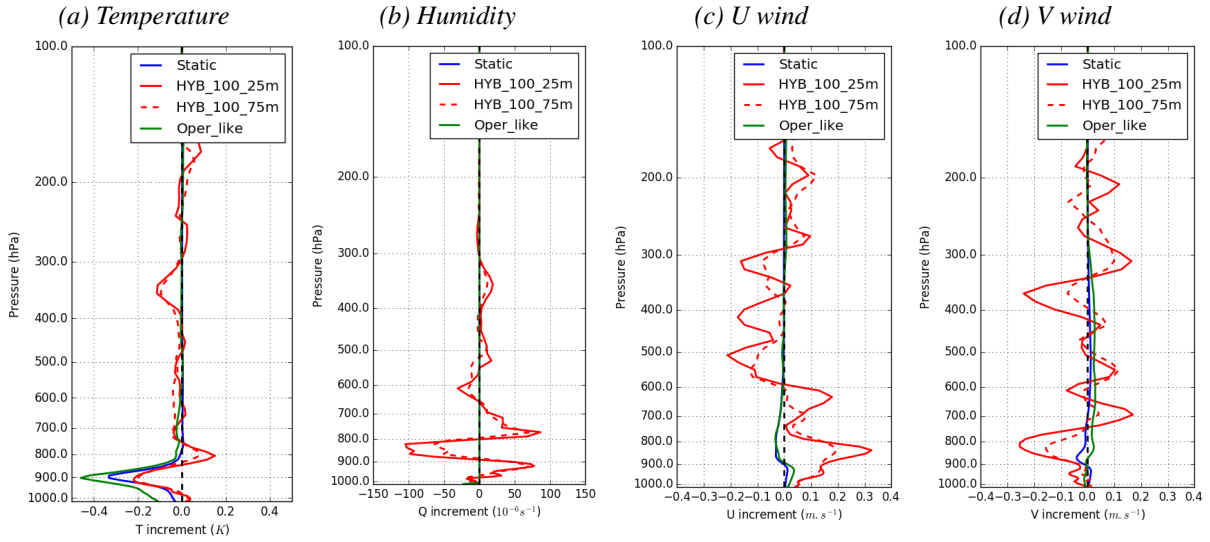

Figure 7: Profiles of increments at the location of the temperature observation for the atmospheric model variables and for different experiments (see Tab. 2 for details).

Figure 7 presents the profiles of the increment for the atmospheric model variables at the location of the observation and for the experiments with a hybrid weight of $\gamma^{e2} = 100\%$. Vorticity and divergence have been replaced by the U and V components of wind. As expected from the above discussion on the increment value at the observation location, the amplitude of the temperature increment from the HYB_100_25m experiment is smaller than for the STATIC and the OPER_LIKE experiments (Fig. 7a). The shape of the increment close to the observation altitude is also different with positive values above the observation altitude in the HYB_100_25m experiment. This positive peak of the temperature increment corresponds to where there are inversions in the temperature profile in the background. The hybrid formulation is able to capture this information.

However, there are vertical fluctuations in the HYB_100_25m experiment at the pressure levels where the two other experiments (STATIC and OPER_LIKE) have a zero-value increment. This is true not only for temperature but for all model variables (Figs. 7b to 7d). This issue is discussed in the following sections.

The profiles of humidity increment also differ a lot between the hybrid experiment on one hand and the STATIC and OPER_LIKE experiments on the other hand. This is due to the balance operator used for these last two experiments (Figs. 8i to 8l). Indeed, the effect of balance operator $\mathbf{K}$ results in putting the humidity increment at the level of the observation away from the observation location, in regions where the background humidity is higher than a threshold and where we have saturation (see Appendix D). In the meantime, the humidity increment of the hybrid experiments is located in the vicinity of the observation location due to the horizontal localisation.

The horizontal localisation in the hybrid experiments also imposes to have the increments of the other variables localised in the vicinity of the observation location (Figs. 8b, 8f, 8n, and 8r). Concurrently, for the OPER_LIKE experiment, significant increments can be found far away, like in the Atlantic ocean (Figs. 8d, 8h, 8p, and 8t). This is the consequence of high (positive or negative) values of the standard deviation in these regions and it can not be avoided in the current formulation of the background errors.

Generally, the horizontal shape of the increments from the hybrid experiments is more anisotropic than the shape the two other experiments (Fig. 8). This could come from both the flow-dependent information and the noise due to the sampling of the background statistics with a small number of members.

4.2 Impact of the time lag in the ensemble members

Increasing the number of members to 75 using the time lag of the EDA members does not change much the temperature increment and the fluctuations above 700 hPa are still present (Fig. 7a). The amplitude of the fluctuations is however smaller with 75 members than with 25 members in the increment profiles of U and V components of wind (Figs. 7c and 7d). In both cases, the increments are still very noisy when compared to the STATIC and OPER_LIKE experiments.

The noise in the profiles is expected for two reasons. First, 25 members or even 75 members are too small a number to have a sufficiently reduced sampling noise. Secondly, we are using the same variables χ^e_m for all the levels and all the variables. With 25 or even 75 of these variables, we may not have enough degrees of freedom to produce a correct increment of temperature around the observation location and a zero increment above 700 hPa for all variables.

Looking at the pressure level of the observation, the noise in the shape of the increments seems to be reduced going from 25 members to 75 members (Fig. 8). This is particularly true for the temperature (Figs. 8b and 8c) and the logarithm of the surface pressure (Figs. 8f and 8g). Most of the increments still keep a more anisotropic shape in the HYB_100_75m experiment than for the STATIC. This means

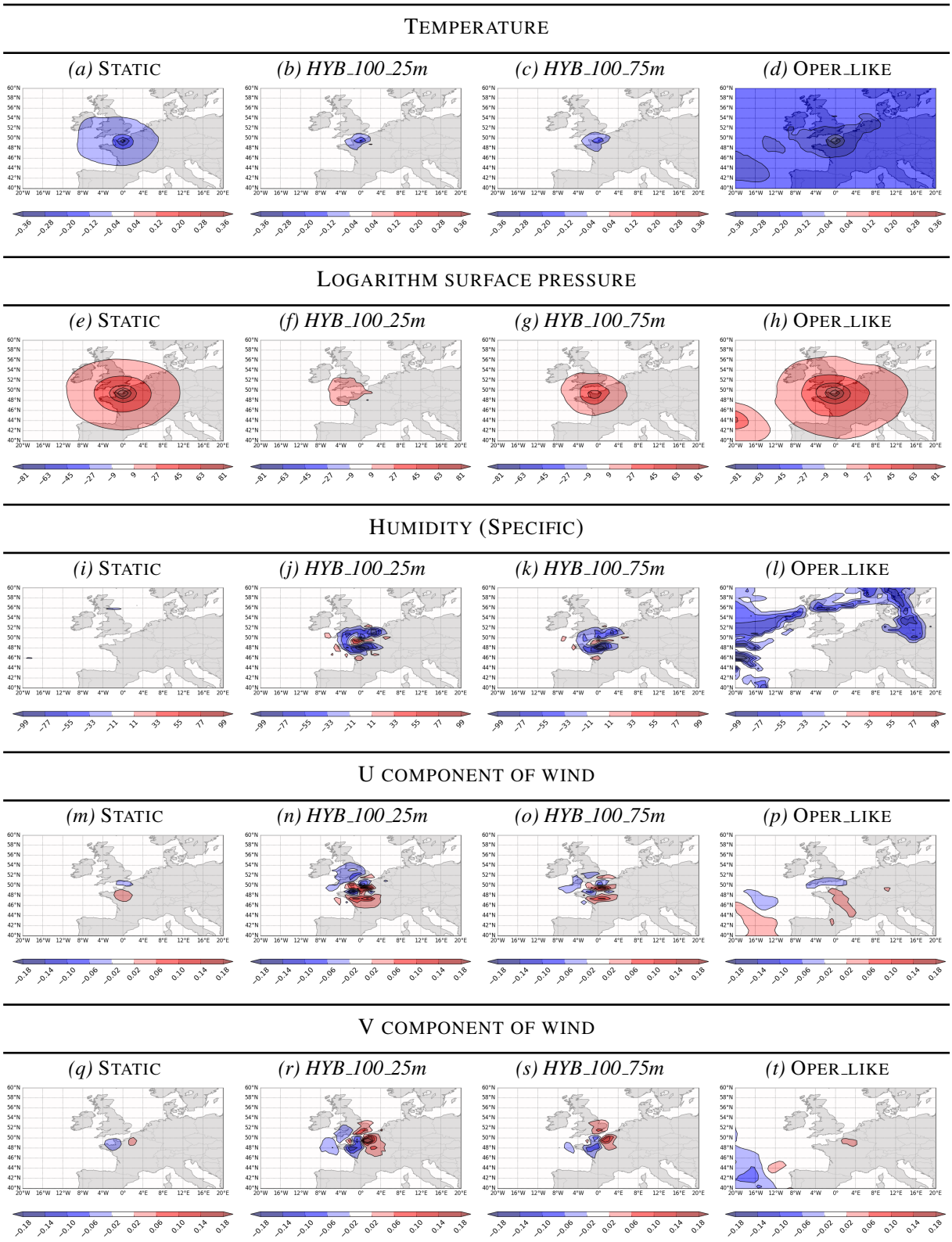

Figure 8: Increments from a single temperature observation located at $(50°N, 0°E)$ *and at about 900* hPa *on 31 October 2016 at 21:00. From top to bottom: temperature (in* K*), logarithm of surface pressure (in* ln(hPa)*), humidity (in* $\mu g.g^{-1}$*), U and V components of wind (in* $m.s^{-1}$*). From left to right: various experiments (see Tab. 2 for more details). All increments are plotted at the model level the closest to 900* hPa *except for the surface pressure.*

that the new hybrid formulation can bring flow-dependent information. Moreover the flow-dependent information is different than the one currently used as the increments between the HYB_100_75m and OPER_LIKE experiments are still significantly different.

4.3 Impact of the hybrid weight

The principle of hybrid background errors is to have a flow-dependent part derived from the ensemble members regularised by a static part. The program *HybridDiag* also provides an optimal weight under the same assumptions used for the optimal localisation (see Section 3.1). With our configuration, *HybridDiag* produces an optimal weight of about $\gamma^{e2} = 75\%$ for the flow-dependent part and with variations lower than 10% between the model levels and the model variables (results not shown). This section discusses the results obtained when the hybrid weight is $\gamma^{e2} = 50\%$ (equal weight) or $\gamma^{e2} = 75\%$ (more weight to the ensemble part and closer to the diagnostic of *HybridDiag*).

Figure 9 presents the new profiles of increment when using 75 members and with the two different hybrid weights. In both cases, the addition of a static component in the background error allows to reduce the unsatisfactory fluctuations in the profiles far from the observation location. Yet, some flow-dependent information is kept in the hybridisation process.

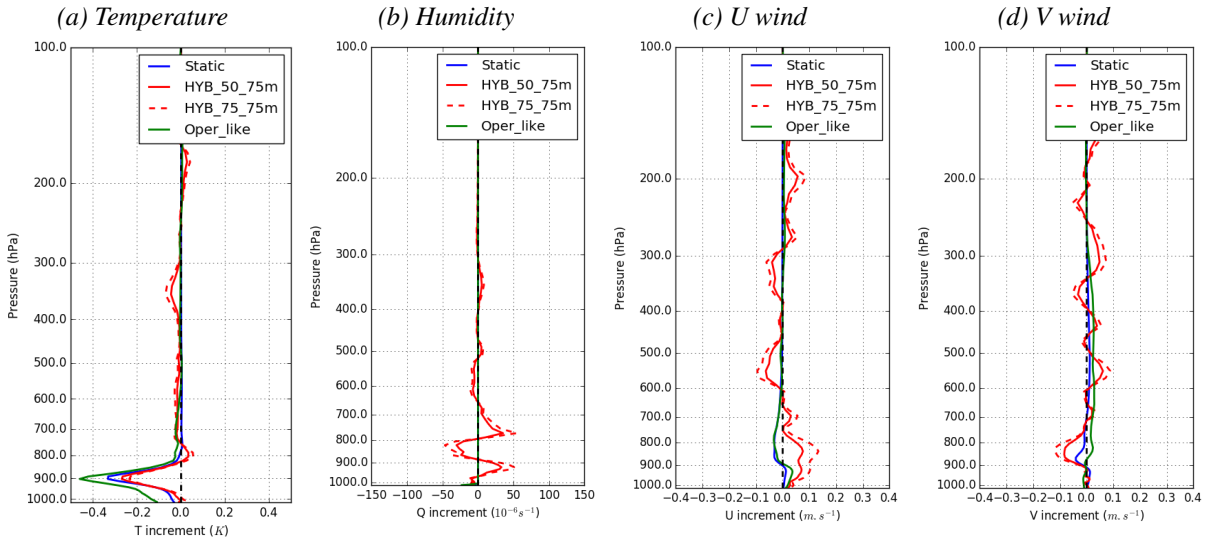

Figure 9: Same as Fig.7 but with different hybrid weights for the hybrid experiments: $\gamma^{e2} = 50\%$ (full red line) and $\gamma^{e2} = 75\%$ (dashed red line).

4.4 Impact of the vertical localisation

In section 2.3 we explained that the chosen implementation of the new hybrid background error formulation disables the possibility to have a vertical localisation. We proposed an alternative to mimic the behaviour of the vertical localisation. For simplicity, hereafter we refer to this alternative solution as vertical localisation.

The vertical localisation should help to further reduce the noise in the increment profiles. It does reduce the noise but it does not help reducing the increment towards zero above 700 hPa (Fig. 10). Moreover the extremes values of the increments are amplified. For example, when the increment of the U com-

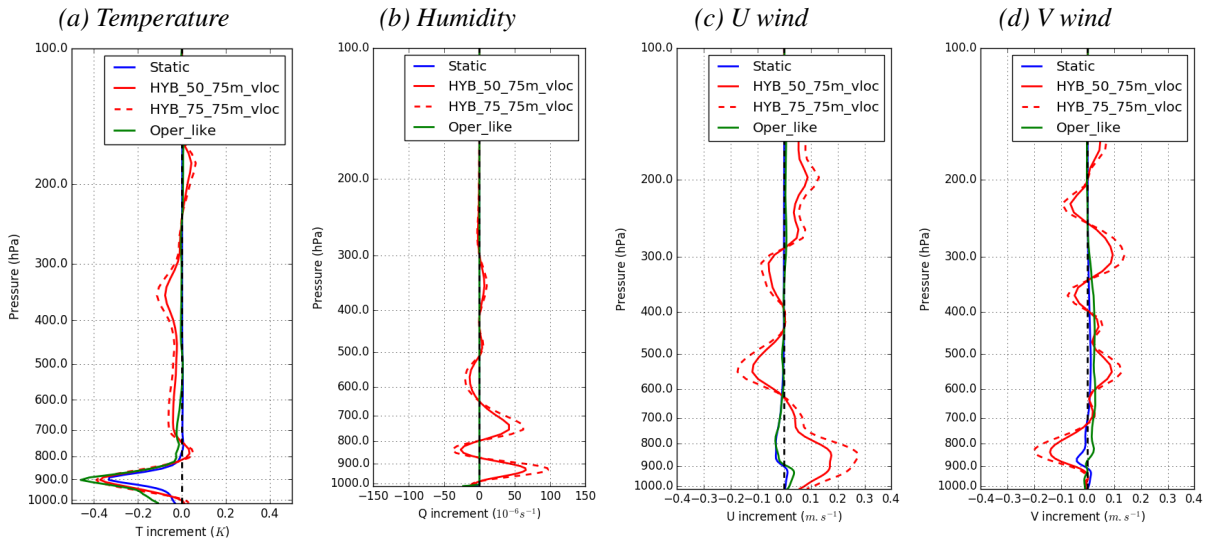

Figure 10: Same as Fig.9 but with vertical localisation for the hybrid experiments.

ponent of wind between 300 hPa and 400 hPa is zero for the STATIC, it is about -0.05 m.s^{-1} in the HYB_500_75m experiment and becomes close to -0.1 m.s^{-1} when using the vertical localisation in the HYB_500_75m_vloc experiment.

These side effects of our implementation of the vertical localisation are expected since we are basically smoothing the increment profiles over few vertical levels. If the raw increment is for example negative over several model levels as for the U component of wind between 300 hPa and 400 hPa (about 8 model levels), then the smoothing over few vertical levels (about 2 model levels) is just producing a smooth version of the raw negative increment. The smoothing is therefore not able to nullify the increment in our case where the vertical localisation length-scale is smaller than the scale of the vertical structures of the noise found in the increments.

5 Summary

In this document we have described a new formulation of the hybrid background errors in the IFS. As in the current approach, the new formulation is hybrid since it combines flow-dependent information and climatological (or static) information. In the new formulation we are making use of the EDA members of the day to directly compute the background errors. The implementation algorithm was described. It consists in augmenting the wavelet control vector with a series of two-dimensional fields χ^e_m, $\forall m \in [1,M]$, where M is the number of used EDA members.

To illustrate the behaviour of the new formulation, we presented the assimilation of a single observation of temperature located at the beginning of the assimilation window. This setting puts emphasis on the background errors. We compared several experiments using the new formulation with two reference experiments that have the same configuration but for the background error. The first reference experiment called STATIC is based on the static background errors which is also used in the new hybrid formulation. The second reference experiment called OPER_LIKE mimics the usage of the background errors of the day we have currently in operations.

In order to reduce the computational cost of the new formulation, the new variables χ^e_m, $\forall m \in [1,M]$ of the control vector are used to account for the background errors of all the atmospheric model variables (divergence, vorticity, temperature, specific humidity and logarithm of surface pressure) and all model levels altogether. This is a strong constraint on the chosen implementation of the new formulation. We showed with the single observation experiment that with this choice the analysis produces unrealistic fluctuations in the profiles of increment far from the observation level. Moreover, this also assumes that the balance between the model variables is correct.

We also showed that we need to apply a localisation to the estimated background errors in order to reduce the sampling noise. We presented some diagnostics of the vertical and horizontal localisation length-scale computed from 10 sets of 25 EDA members. The diagnostics suggest very different horizontal length-scales for the atmospheric model variables of which we want to represent the background errors. We thus propose a transformation of the EDA members based on the Laplacian operator. The localisation is one obvious advantage of the new formulation since it constrains the increment to be in the vicinity of the observation while in the current approach large increments could be found far away from the observation location for some atmospheric model variables.

With the chosen implementation of the new hybrid background errors, the two-dimensional fields χ^e_m are valid for all model levels. Therefore we can not have a vertical localisation. Instead we propose to mimic the behaviour of the vertical localisation by applying a correlation function on the vertical increment. We showed that this implementation is effective in smoothing the profiles of increment but ineffective in removing the unrealistic fluctuations in the profiles. Therefore the usefulness of this should be revisited when a full set of observation is assimilated. We should also investigate in parallel the implementation using three-dimensional fields χ^e_m. This would increase the size of the control vector by too much and methods to reduce the size should be explored.

To reduce the sampling noise, we increased by a factor of three the number of used members by using the EDA members shifted in time by ± 3 hour. We showed that this helps to reduce the noise, especially regarding the horizontal shape of the increment. Even though this proves to be helpful, this is not completely satisfactory. In case of local events like tropical cyclones, the local covariance could change rapidly during a time window of 6 hours. The next step would be to use a time lag of ± 1 hour instead of ± 3 hour. In parallel, we are running some tests of an EDA with 50 members instead of 25 members. We plan to rerun the diagnostics of the localisation on the 50 members and to assess if we need the time lag or not.

By tripling the number of members in the new formulation, we could reduce the unrealistic fluctuations in the profiles of increment far from the observation level. We reduced them further with the hybridisation of the background error. By adding already 25% of static error, the noise is indeed greatly reduced. We now have to run experiments with the full observing system and over a long period, and with various hybrid weights to assess the optimal value of the weight.

Before running experiments over a long period of time, we need to (i) test the assimilation of the full observing system and (ii) test the implementation in a configuration with several outer loops. We already tested the assimilation of the full observing system and the results are encouraging. We are currently working on the implementation of the outer loop facility. The choice of the resolution of the perturbations as well as the choice of the localisation length-scale for each loop have to be investigated.

The strongest assumption of our implementation of the new formulation for the hybrid background errors in the IFS is the choice of the same χ^e_m variables for all model levels and for all model variables. For the longer term developments, we could imagine having different set of χ^e_m variables for different part of the atmosphere (boundary layer, free troposphere and stratosphere) or different set of model variables

(physical variables and chemical variables like ozone). For that, more work is needed on the balance between the model variables and in particular to decide if we should apply the localisation on the balanced or unbalanced variables.

Regarding the horizontal localisation, the current implementation assumes a constant length-scale in space. We choose the wavelet approach for the implementation of the horizontal localisation to be able to have a localisation with a length-scale that varies spatially and that could also vary with the wavenumber. The benefit of using such a localisation will be assessed in the near future.

6 Acknowledgements

The author would like to thank Massimo Bonavita (ECMWF), Elias Hólm (ECMWF) and Loïk Berre (Météo-France) for their comments and advice during the production of this document.

HybridDiag is a very useful tool when it comes to do hybridisation of background errors. It was used quite a lot in this document. Many thanks to Benjamin Ménétrier (Météo-France) for this software and for his help adapting *HybridDiag* for our needs.

The author would also like to thank Gérald Desroziers (Météo-France, now retired) and Antony Weaver (Cerfacs) for all the discussions around the hybridisation of background errors.

Bibliography

Berre, L., Arbogast, E., Ménétrier, B., and Desroziers, G. (2017). Change of variable applied to mass and wind fields for covariance localisation. WMO CAS/JSC WGNE Blue Book, Edited by J. Côté.

Bonavita, M., Isaksen, L., and Hólm, E. (2012). On the use of EDA background error variances in the ECMWF 4D-Var. *Q.J.R. Meteorol. Soc.*, 138(667):1540–1559.

Desroziers, G., Camino, J.-T., and Berre, L. (2014). 4DEnVar: link with 4D state formulation of variational assimilation and different possible implementations. *Q.J.R. Meteorol. Soc.*, 140(684):2097–2110.

Fisher, M. and Andersson, E. (2001). Developments in 4D-Var and Kalman Filtering. ECMWF Technical Memorandum No. 347.

Gaspari, G. and Cohn, S. (1999). Construction of correlation functions in two and three dimensions. *Q.J.R. Meteorol. Soc.*, 125(554):723–757.

Hamill, T. M. and Snyder, C. (2000). A Hybrid Ensemble Kalman Filter–3D Variational Analysis Scheme. *Monthly Weather Review*, 128(8):2905–2919.

Ménétrier, B. and Auligné, T. (2015). Optimized localization and hybridization to filter ensemble-based covariances. *Monthly Weather Review*, 143(10):3931–3947.

Rochas, M. and Courtier, P. (1992). La méthode spectrale en météorologie. Note de travail ARPEGE No. 30. Toulouse: Météo-France.

Weaver, A. T. and Mirouze, I. (2013). On the diffusion equation and its application to isotropic and anisotropic correlation modelling in variational assimilation. *Q.J.R. Meteorol. Soc.*, 139(670):242–260.

Appendix A Computation of the vertical correlation in the wavelet space

The background error correlation operator in the IFS is formulated in the wavelet space. For that purpose, a vertical correlation matrix is computed for each "cutoff" wavenumber N_j of the wavelet decomposition, with $j \in [0,J]$. As explained in the section 1.2, each wavenumber N_j is associated with its own horizontal grid. These horizontal grids are currently all coarser than the horizontal grid used in the EDA. As a consequence, we have several cells of the EDA grid G_e included in a cell of the grid G_j associated with the wavenumber N_j for any $j \in [0,J]$.

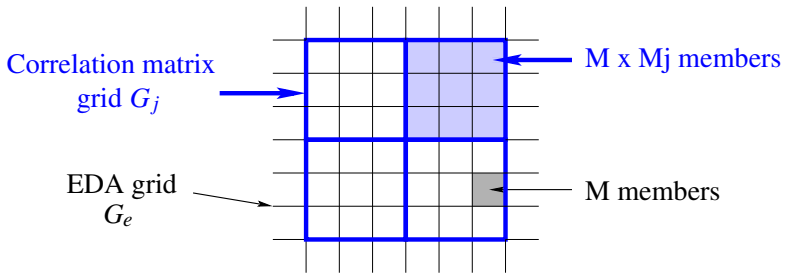

Figure A.1: Basic example of a horizontal grid used for the correlation matrix with the wavelet formulation (blue) and the horizontal grid used for the EDA (black). In this example, we have M_j=9 grid cells of the EDA grid included in G_j (blue shade).

For each cell of G_e, we have M members from the EDA and thus M samples of the background. If M_j is the number of grid cells of G_e included in G_j, them we have $M \times M_j$ samples per grid cell of G_j (Fig. A.1). Let us denote $x^{ub}_{k,m,t}$ the m^{th} element of vector composed with all the unbalanced background vectors included in G_j and for the level k and time t. The index m belongs to the interval $[1, M \times M_j]$ and therefore depends on the wavenumber N_j, but the dependence is omitted for simplicity.

The sample is further increased using not only the EDA members at the analysis time but also the members with times around the analysis time. Currently we are using a time-lag up to 3 hour and a time-step of 1 hour. This corresponds to a number of times equal to $M_t = 7$.

We are using the $M \times M_j \times M_t$ samples of the background to compute a vertical correlation matrix of the background error in each cell of G_j. For instance, the element of the column k and row l of this matrix is the correlation between the model levels k and l and is computed as

$$c^e_j(k,l) = \frac{1}{\sigma^v_k \sigma^v_l} \sum_{t=1}^{M_t} \sum_{m=1}^{M \times M_j} \left(x^{ub}_{k,m,t} - \overline{x^{ub}_k} \right) \left(x^{ub}_{l,m,t} - \overline{x^{ub}_l} \right) , \tag{36}$$

where $\bar{\cdot}$ denotes the mean and σ the standard deviation, both computed using the $M \times M_j \times M_t$ samples.

Appendix B Two-dimensional augmented variable

The new hybrid formulation requires to compute the product of the square root of the ensemble-based localised background error $\mathbf{B}^e$ with the augmented part of the control vector χ^e as

$$\mathbf{B}^{e\,\frac{1}{2}}\, \chi^e = \widehat{D}\widehat{C}^{\frac{1}{2}}\, \chi^e , \tag{37}$$

where $\widehat{D}$ and $\widehat{C}$ are detailed in section 2.3. Here, χ^e has the dimension $M \times (n_{3D} n_l + n_{2D}) \times \text{size}(\chi_w)$ (using notation from section 2.3.2). For simplicity in the notations, we define $N_w = \text{size}(\chi_w)$.

We assume that the M variables χ_m^e, $\forall m \in [1,M]$, are not correlated to each other. We also assume that the localisation is the same for each χ_m^e variable. In that case $\widehat{C}^{\frac{1}{2}}$ is block diagonal and each block is identical to each other and we refer to it as $\widehat{C}_\chi^{\frac{1}{2}}$

$$\widehat{C}^{\frac{1}{2}}\,\chi^e = \begin{pmatrix} \widehat{C}_\chi^{\frac{1}{2}}\chi_1^e \\ \widehat{C}_\chi^{\frac{1}{2}}\chi_2^e \\ \ddots \\ \widehat{C}_\chi^{\frac{1}{2}}\chi_M^e \end{pmatrix}, \tag{38}$$

In order to reduce the cost of the new method, we decided to have the same χ_m^e variables for each control variables and for each level of the control variable. We call this new variables $\tilde{\chi}_m^e$, $\forall m \in [1,M]$ and the transformation from $\tilde{\chi}_m^e$ towards χ_m^e is done through the operator Θ,

$$\chi_m^e = \Theta\,\tilde{\chi}_m^e\,. \tag{39}$$

Note that for each $m \in [1,M]$ the dimension of $\tilde{\chi}_m^e$ is N_w while the dimension of χ_m^e is $(n_{3D}\,n_l + n_{2D}) \times N_w$. If $\mathbf{1}$ and $\mathbf{0}$ are vectors of dimension $(n_{3D}\,n_l + n_{2D})$, respectively filled with 1 and 0, then the matrix Θ becomes

$$\Theta = \begin{pmatrix} \mathbf{1} & \mathbf{0} & \cdots & \\ \mathbf{0} & \mathbf{1} & \mathbf{0} & \\ & & \ddots & \\ & \cdots & \mathbf{0} & \mathbf{1} \end{pmatrix}. \tag{40}$$

Using the transformation by Θ each bock of the $\widehat{C}_\chi^{\frac{1}{2}}\chi_m^e$ matrix of Eq. (38) becomes

$$\widehat{C}_\chi^{\frac{1}{2}}\chi_m^e = \widehat{C}_\chi^{\frac{1}{2}}\Theta\tilde{\chi}_m^e\,. \tag{41}$$

With the hypothesis that $\tilde{\chi}_m^e$, $\forall m \in [1,M]$, is the same for all vertical levels, there is no sense to have vertical correlation. If we assume that the horizontal correlation is the same for each $\tilde{\chi}_m^e$ variables and if $\widehat{C}_h^{\frac{1}{2}}$ denotes this $N_w \times N_w$ horizontal correlation, then the previous equation could be rewritten

$$\widehat{C}_\chi^{\frac{1}{2}}\chi_m^e = \Theta\widehat{C}_h^{\frac{1}{2}}\tilde{\chi}_m^e\,. \tag{42}$$

Note that we have commuted the correlation operator and the Θ operator. This means that for each member $m \in [1,M]$, we apply the horizonal localisation of the variable $\tilde{\chi}_m^e$ and then we can propagate this on all variables and all levels. This can be extended to the initial product of Eq. (37) using the particular form of $\widehat{D}$ from Eq. (24),

$$\mathbf{B}^{e\,\frac{1}{2}}\chi^e = \sum_{m=1}^{M} x_m^{b'} \circ \Theta\widehat{C}_h^{\frac{1}{2}}\,\tilde{\chi}_m^e\,. \tag{43}$$

Appendix C Single observation experiment

In this appendix, we want to document the impact of the correlation length-scale and the impact of the interpolation of the observation location on the increment in the case of a single observation. To simplify

the problem, we assume the one-dimensional case where the observation operator $\mathbf{H}$ consists only in a space interpolation. If the location of the observation y is between the grid-points k and $k+1$ and if we perform a linear interpolation between the two grid-points, then the observation operator if full of zeros but for its indexes k and $k+1$,

$$\mathbf{H} = \Big(\underset{k-1}{0}, \quad \cdots, \quad \underset{k}{0}, \quad \underset{k}{1-\alpha}, \quad \underset{k+1}{\alpha}, \quad 0, \quad \cdots, \quad 0 \Big) . \tag{44}$$

The parameter α is for the linear interpolation. A value of 1 would mean that the observation is exactly on the grid-point k. A value of 0.5 would mean that the observation is exactly in between the two grid-points k and $k+1$.

The analysis increment $\delta\mathbf{x}_a = \mathbf{x}_a - \mathbf{x}_b$ given by the best linear unbiased estimate is

$$\delta\mathbf{x}_a = \mathbf{K}\left(\mathbf{y} - \mathbf{H}\mathbf{x}_b\right) , \tag{45}$$

where $\mathbf{x}_a$ is the analysis, $\mathbf{x}_b$ is the background. The operator $\mathbf{K}$ is the gain matrix that can be expressed as a function of the observation operator, the background error covariance matrix $\mathbf{B}$ and the observation error covariance matrix $\mathbf{R}$,

$$\mathbf{K} = \mathbf{B}\mathbf{H}^{\mathrm{T}} \left[\mathbf{H}\mathbf{B}\mathbf{H}^{\mathrm{T}} + \mathbf{R}\right]^{-1} . \tag{46}$$

For this example, we assume that the background error are Gaussian with a standard deviation σ_b^2, and a correlation length-scale L. The element (i,j) of $\mathbf{B}$ is denoted $b_{i,j}$ and is expressed as

$$b_{i,j} = \sigma_b^2 \, c_{i,j} \tag{47}$$

$$= \sigma_b^2 \, e^{-\frac{(\|i-j\|\delta x)^2}{2L^2}} , \tag{48}$$

In this one-dimensional case, the $\mathbf{B}\mathbf{H}^{\mathrm{T}}$ matrix become a vector, and its i^{th} element is

$$\left(\mathbf{B}\mathbf{H}^{\mathrm{T}}\right)_i = (1-\alpha)\, b_{i,k} + \alpha\, b_{i,k+1} . \tag{49}$$

If we left-multiply this $\mathbf{B}\mathbf{H}^{\mathrm{T}}$ vector by $\mathbf{H}$, we compute the scalar

$$\mathbf{H}\mathbf{B}\mathbf{H}^{\mathrm{T}} = (1-\alpha)\left[(1-\alpha)\, b_{k,k} + \alpha\, b_{k,k+1}\right] + \alpha\left[(1-\alpha)\, b_{k+1,k} + \alpha\, b_{k+1,k+1}\right] \tag{50}$$

$$= \sigma_b^2 \left[(1-\alpha)^2 + 2\,\alpha\,(1-\alpha)\, c_{k,k+1} + \alpha^2\right] . \tag{51}$$

Adding to this the observation error $\mathbf{R} \equiv \sigma_o^2$ for the single observation, we have the denominator part of the gain matrix.

To compute the analysis increment, we first need to compute the innovation $d = y - \mathbf{H}\mathbf{x}_b$. With the particular form of $\mathbf{H}$, we have

$$d = y - \left[(1-\alpha)\,(\mathbf{x}_b)_k + \alpha\,(\mathbf{x}_b)_{k+1}\right] , \tag{52}$$

where $(\mathbf{x}_b)_k$ and $(\mathbf{x}_b)_{k+1}$ are respectively the k^{th} and $(k+1)^{th}$ elements of the background vector $\mathbf{x}_b$.

We are interested in how the increment at the closest grid point to the analysis evolves with the interpolation coefficient α or the length-scale of the background error correlation. From the analysis increment $\delta\mathbf{x}_a$, we extract the k^{th} element

$$(\delta\mathbf{x}_a)_k = \frac{\sigma_b^2 \left[(1-\alpha) + \alpha\, e^{-\frac{\delta x^2}{2L^2}}\right]}{\sigma_o^2 + \sigma_b^2 \left[(1-\alpha)^2 + 2\,\alpha\,(1-\alpha)\, e^{-\frac{\delta x^2}{2L^2}} + \alpha^2\right]} d \tag{53}$$

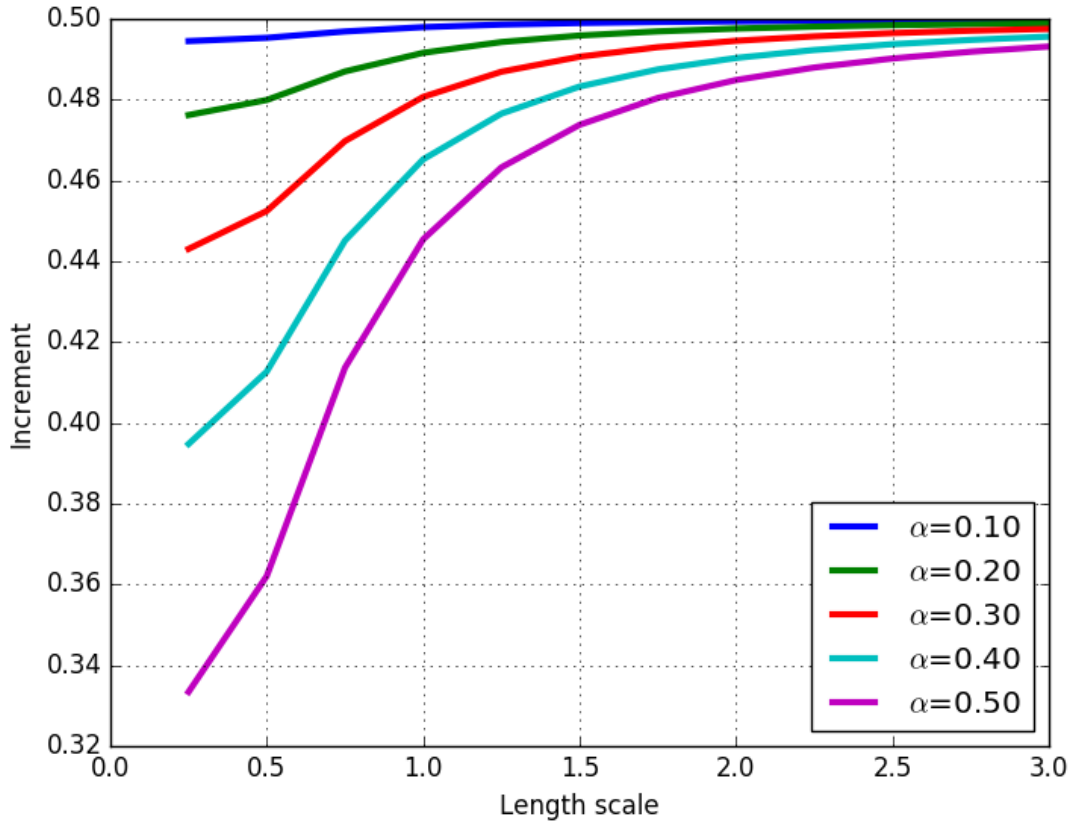

Figure C.1: Impact of the interpolation coefficient α and of the length-scale $\frac{L}{\delta x}$ of the background error correlation on the analysis increment in the grid point the closest to the single observation.

Figure C.1 presents the sensitivity of $(\delta \mathbf{x}_a)_k$ of Eq.(53) with α and L in the particular case where $\sigma_b^2 = \sigma_o^2$ and the innovation d of Eq.(52) is independent of α (true if $(\mathbf{x}_b)_k = (\mathbf{x}_b)_{k+1}$) and equal to 1.

First of all, if the observation is located exactly on the grid point corresponding to the index k, then $\alpha = 0$. The analysis increment in that grid point is independent to the length-scale of the background error correlation and is equal to 0.5 in our particular configuration.

For a given $\alpha \neq 0$, the analysis increment in the nearest grid point of the observation tends to 0.5 when the length-scale of the background error correlation increases. For an observation in the middle of two grid points ($\alpha = 0.5$) and a length-scale of the background error correlation of the same order of the grid point, then the increment is about 0.44.

Appendix D Saturation adjustment and humidity increment

In the current formulation of the balance operator **K**, the saturation adjustment is active when the relative humidity is larger than a threshold of 80%. In that situation, a temperature increment is spread into a specific humidity increment. For the single observation experiment presented in this document, the observation is located in a region where the relative humidity is lower than 80% (Fig. D.1a).

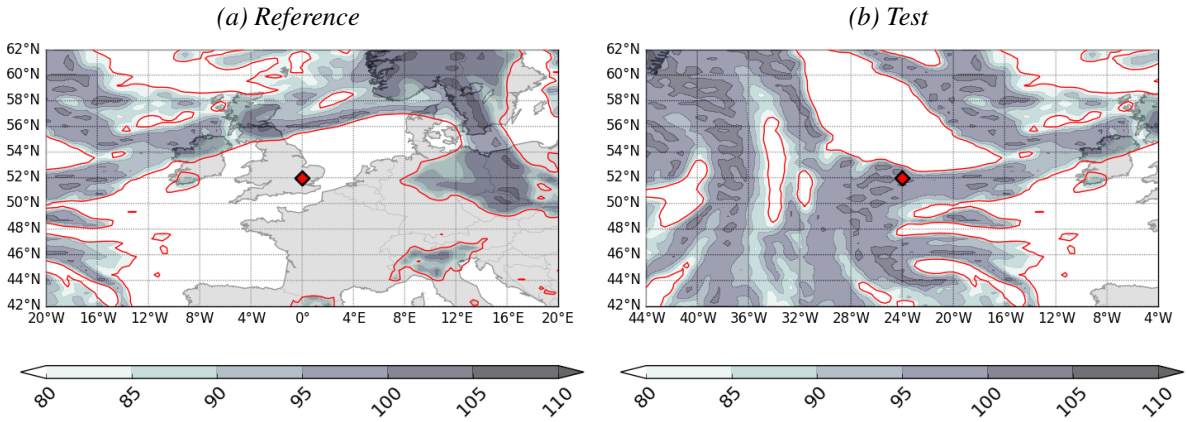

Figure D.1: Background values of relative humidity (in %) for two regions at 900 hPa *(grey shade). The red line is the 80% contour value which is the selected threshold for the saturation adjustment, and the red diamond represents the localisation of the observation.*

In the OPER_LIKE experiment, the temperature increment still has significant values in regions far from the observation location but where the relative humidity is larger than 80% (Fig. 8d, page 18). This results in specific humidity increments that have a similar shape as the relative humidity above 80% (Fig. 8l, page 18 and Fig. D.1a). We have a similar effect for the STATIC experiment, but the values of the specific humidity increment are smaller than for the OPER_LIKE experiment. Indeed, values of the temperature increment are also smaller in the regions where we have the saturation adjustment.

We also ran another single observation set of experiments for an observation located in a region where the relative humidity is larger than 80%, at the coordinates $(52.28°N, 24.0°W)$ (Fig. D.1b). Figure D.2 presents the resulting increments for temperature and humidity only and for similar experiments as before. Note that for this case, there is no rescaling of the standard deviation of the background error in the STATIC experiment. Yet, the temperature increments have a similar amplitude for all experiments. The saturation adjustment is now active around the location of the observation and therefore the specific humidity increment is localised in the surroundings of the observation location in the OPER_LIKE and the STATIC experiments. Interestingly, the specific humidity increment has the opposite sign for the experiments with the new hybrid formulation of the background error and with larger (opposite) values too. This response of specific humidity to temperature increment is currently under investigation and work is in progress to improve the balance operator.

TEMPERATURE

(a) STATIC *(b) HYB_50_75m* *(c) HYB_100_75m* *(d)* OPER_LIKE

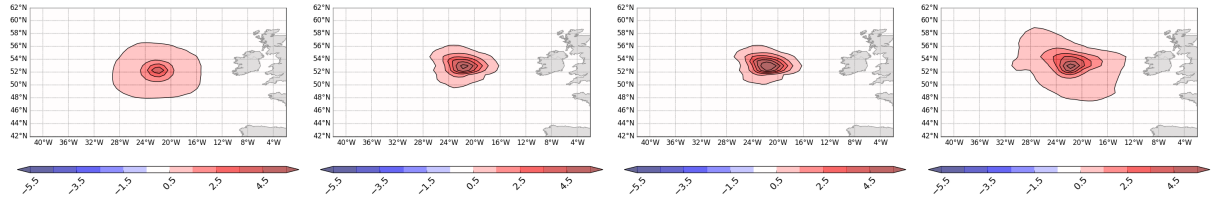

HUMIDITY (SPECIFIC)

(e) STATIC *(f) HYB_50_75m* *(g) HYB_100_75m* *(h)* OPER_LIKE

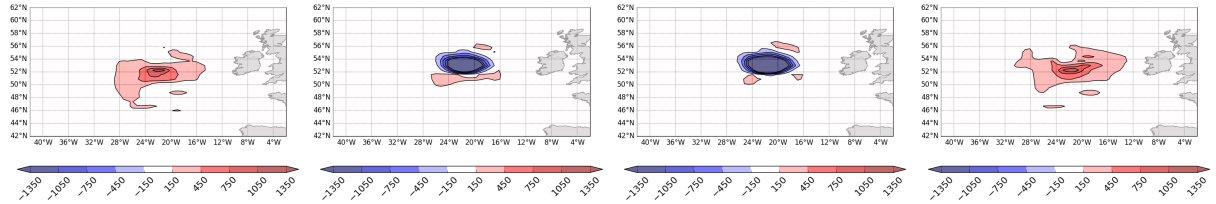

Figure D.2: Same as Fig. 8 but for a temperature observation located in a region where the relative humidity is larger than 80% $(52°N, 24°W)$.